Communication between Remote Moieties in Linear Ru−Ru−Ru Trimetallic Cyanide-Bridged Complexes

German E. Pieslinger,[†] Pablo Albores,[†] Leonardo D. Slep,[†] Benjamin J. Coe,[§] Cliff J. Timpson,[⊥] and Luis M. Baraldo*,[†]

[†]Departamento de Química Inorgánica, Analítica y Química Física, INQUIMAE-CONICET, Facultad de Ciencias Exactas y Naturales, Universidad de Buenos Aires, Pabellón 2, 3 piso, Ciudad Universitaria, C1428EHA Buenos Aires, Argentina

[§]Department of Chemistry, University of Manchester, Oxford Road, Manchester M13 9PL, U.K.

[⊥]Department of Chemistry and Physics, Roger Williams University, 1 Old Ferry Road, Bristol, Rhode Island 02809, United States

S *Supporting Information*

ABSTRACT: In this article, we report the structural, spectroscopic, and electrochemical properties of the cyanide-bridged complex salts *trans*-[(NC)Ru^{II}(L)$_4$(μ-CN)Ru^{II}(py)$_4$Cl]PF$_6$ and *trans*-[Ru^{II}(L)$_4${(μ-CN)-Ru^{II}(py)$_4$Cl}$_2$](PF$_6$)$_2$ (L = pyridine or 4-methoxypyridine). The mixed-valence forms of these compounds show a variety of metal-to-metal charge-transfer bands, including one arising from charge transfer between the remote ruthenium units. The latter is more intense when L = 4-methoxypyridine and points to the role of the bridging ruthenium unit in promoting mixing between the dπ orbitals of the terminal fragments.
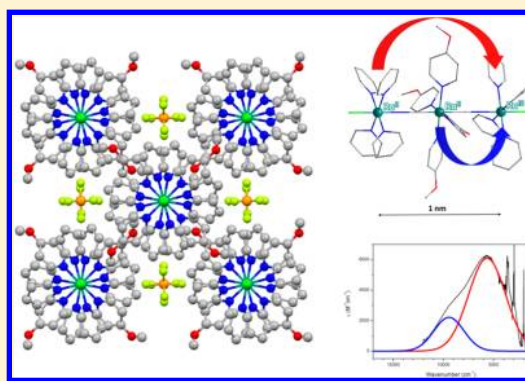
INTRODUCTION

Cyanide-bridged complexes have been explored extensively, and clusters of different geometries and nuclearities,[1−5] including large systems like nanoparticles[6] and surfaces,[7] have been reported. One of the motivations for this exploration is the ability of the cyanide bridge to promote a strong coupling between metallic fragments, which results in interesting magnetic and spectroscopic properties.[1−10] More than 15 years ago, Coe et al. reported the syntheses of two interesting multimetallic linear complex salts, *trans*-[(NC)Ru^{II}(py)$_4$(μ-CN)Ru^{II}(py)$_4$Cl]PF$_6$ and *trans*-[Ru^{II}(py)$_4${(μ-CN)-Ru^{II}(py)$_4$Cl}$_2$](PF$_6$)$_2$.[11] The latter complex salt shows that the *trans*-[Ru^{II}(CN)$_2$(py)$_4$] fragment promotes electronic coupling between the terminal [Ru^{II}(py)$_4$Cl]$^+$ units, as evidenced by the observed difference of 100 mV between their ruthenium(III/II)-associated redox potentials.[12] This coupling is also reflected in the electronic spectroscopy of the different redox states of these two compounds, particularly in the properties of their observed metal-to-metal charge-transfer (MMCT) transitions.[13]

We report here the related new compounds *trans*-[Ru^{II}(CN)$_2$(MeOpy)$_4$], *trans*-[(NC)Ru^{II}(MeOpy)$_4$(μ-CN)-Ru^{II}(py)$_4$Cl]PF$_6$, and *trans*-[Ru^{II}(MeOpy)$_4${(μ-CN)-Ru^{II}(py)$_4$Cl}$_2$](PF$_6$)$_2$, including the structural crystallographic characterization of the latter. Ascertaining the effects of replacing some of the pyridine (py) ligands with the more basic 4-methoxypyridine (MeOpy) is of particular interest. For comparison purposes, we also report the spectroscopic

properties of *trans*-[(NC)Ru^{II}(py)$_4$(μ-CN)Ru^{II}(py)$_4$Cl]PF$_6$, *trans*-[Ru^{II}(py)$_4${(μ-CN)Ru^{II}(py)$_4$Cl}$_2$](PF$_6$)$_2$, and their oxidized forms, including new IR data. A summary of all of the complexes studied is shown in Scheme 1.

EXPERIMENTAL SECTION

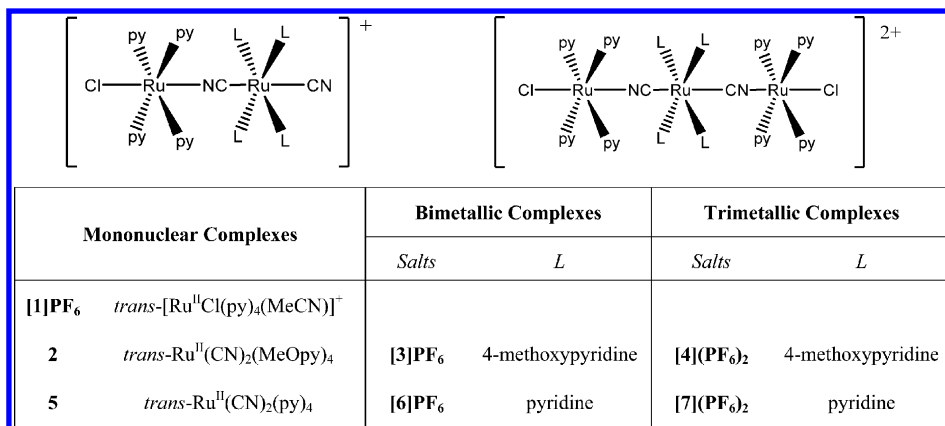**Materials.** The compounds *trans*-[Ru^{II}(CN)$_2$(py)$_4$] (**5**),[14] *trans*-[Ru^{II}Cl$_2$(MeOpy)$_4$],[15] *trans*-[Ru^{II}Cl(py)$_4$(NO)](PF$_6$)$_2$,[14] *trans*-[(NC)Ru^{II}(py)$_4$(μ-CN)Ru^{II}(py)$_4$Cl]PF$_6$ (**[6]**PF$_6$),[11] and *trans*-[Ru^{II}(py)$_4${(μ-CN)Ru^{II}(py)$_4$Cl}$_2$](PF$_6$)$_2$ (**[7]**(PF$_6$)$_2$)[11] were prepared according to previously published procedures. Solvents for UV−visible and electrochemistry measurements were dried according to literature procedures.[16] Tetra-*N*-butylammonium hexafluorophosphate, [TBA]-PF$_6$ (Aldrich), used in the cyclic voltammetry experiments was recrystallized from ethanol. All other reagents were obtained commercially and used as supplied. The new compounds synthesized were dried in a vacuum desiccator for at least 12 h prior to characterization.

Synthesis of *trans*-[Ru^{II}Cl(py)$_4$(MeCN)]PF$_6$ ([1]PF$_6$). This compound was prepared by a route different from that previously published.[17] A solution of *trans*-[Ru^{II}Cl(py)$_4$(NO)](PF$_6$)$_2$ (97 mg, 0.126 mmol) and NaN$_3$ (9 mg, 0.138 mmol) in acetonitrile (10 mL) was stirred at room temperature for 2 h under an argon atmosphere. Acetonitrile was evaporated, and the addition of aqueous NH$_4$PF$_6$ afforded a yellow precipitate. This solid was collected by filtration, washed with water, and dried. Purification was effected by acetone elution of an alumina column and collection of the major yellow band.

Scheme 1. Structures of the Ruthenium Complexes Studied in This Work

Mononuclear Complexes		**Bimetallic Complexes**		**Trimetallic Complexes**	
		Salts	*L*	*Salts*	*L*
[**1**]PF$_6$	*trans*-[Ru^{II}Cl(py)$_4$(MeCN)]$^+$				
2	*trans*-Ru^{II}(CN)$_2$(MeOpy)$_4$	[**3**]PF$_6$	4-methoxypyridine	[**4**](PF$_6$)$_2$	4-methoxypyridine
5	*trans*-Ru^{II}(CN)$_2$(py)$_4$	[**6**]PF$_6$	pyridine	[**7**](PF$_6$)$_2$	pyridine

The product was then recrystallized from acetonitrile/diethyl ether to afford a yellow solid. Yield: 62 mg, 77%. Anal. Calcd for C$_{22}$H$_{23}$ClF$_6$N$_5$PRu: C, 41.4; H, 3.6; N, 11.0. Found: C, 41.0; H, 3.8; N, 10.3. ^{1}H NMR (CD$_3$COCD$_3$, δ_H/ppm): 8.47 (8H, d, H^{2,6} × 4), 7.93 (4H, t, H^4 × 4), 7.36 (8H, t, H^{3,5} × 4), 2.81 (3H, s, CH$_3$).

Synthesis of *trans*-[Ru^{II}(CN)$_2$(MeOpy)$_4$] (2). *trans*-[Ru^{II}Cl$_2$(MeOpy)$_4$] (1.59 g, 2.61 mmol) and KCN (3.47 g, 53.2 mmol) were suspended in methanol (250 mL) and refluxed for 3 h. The clear orange solution was evaporated to dryness, yielding a yellow solid, and unreacted KCN was removed by washing with abundant water. The yellow solid was then dried under vacuum to yield 1.23 g (80%) of pure product. Anal. Calcd for C$_{26}$H$_{28}$N$_6$O$_4$Ru: C, 53.0; H, 4.8; N, 14.3. Found: C, 52.9; H, 4.7; N, 13.9. ^{1}H NMR (CD$_3$OD, δ_H/ppm): 8.37 (8H, d, H^{2,6} × 4), 6.79 (8H, d, H^{3,5} × 4), 3.85 (12H, s, OCH$_3$ × 4). IR (KBr): ν(CN) 2056 (s) cm^{-1}.

Synthesis of *trans*-[(NC)Ru^{II}(MeOpy)$_4$(μ-CN)Ru^{II}(py)$_4$Cl]PF$_6$ ([3]PF$_6$). *trans*-[Ru^{II}Cl(py)$_4$(NO)](PF$_6$)$_2$ (106 mg, 0.138 mmol) and NaN$_3$ (9.7 mg, 0.149 mmol) were allowed to react in acetone (5 mL) under an argon atmosphere and protected from the light to yield the solvent complex [Ru^{II}Cl(py)$_4$(Me$_2$CO)]$^+$. After 1 h, half of the solvento complex was anaerobically transferred, dropwise and with constant stirring, into a solution of **2** (679 mg, 1.15 mmol) in deaerated methanol (15 mL). This mixture was allowed to react for 30 min, and then the remaining solvento species was added slowly and allowed to react for a further 30 min. Solvents were removed under vacuum, and the resulting yellow solid was suspended in acetonitrile (10 mL). The insoluble excess of **2** was removed by filtration. The yellow solution was evaporated to dryness, the solid was dissolved in acetone (2 mL), and saturated aqueous NH$_4$PF$_6$ was added. After standing overnight at 4 °C, the yellow solid was collected by filtration, washed with chilled water, and dried under vacuum. Purification was accomplished through a short column of alumina (dimensions 15 × 2 cm) in acetone, followed by recrystallization from acetone/water. Yield: 98 mg, 60%. Anal. Calcd for C$_{46}$H$_{48}$ClF$_6$N$_{10}$PO$_4$Ru$_2$·CH$_3$COCH$_3$: C, 47.3; H, 4.4; N, 11.3. Found: C, 47.0; H, 4.3; N, 11.2. ^{1}H NMR (CD$_3$COCD$_3$, δ_H/ppm): 8.33 (8H, s, H$^{2,6}_{py}$ × 4), 8.14 (8H, d, H$^{2,6}_{MeOpy}$ × 4), 7.80 (4H, t, H$^4_{py}$ × 4), 7.08 (8H, t, H$^{3,5}_{py}$ × 4), 6.54 (8H, d, H$^{3,5}_{MeOpy}$ × 4), 3.85 (12H, s, OCH$_3$ × 4). IR (KBr): ν(CN) 2058 (s) cm^{-1}.

Synthesis of *trans*-[Cl(py)$_4$Ru^{II}(μ-NC)Ru^{II}(MeOpy)$_4$(μ-CN)-Ru^{II}(py)$_4$Cl](PF$_6$)$_2$ ([4](PF$_6$)$_2$). A solution of *trans*-[Ru^{II}Cl(py)$_4$(NO)]-(PF$_6$)$_2$ (200 mg, 0.259 mmol) and NaN$_3$ (17.8 mg, 0.274 mmol) in deaerated acetone (10 mL) was stirred at room temperature for 1 h. Solid **2** (75 mg, 0.127 mmol) was added, and the solution was stirred in the dark for a further 3 days. The addition of water (50 mL) afforded a mustard-yellow precipitate, which was collected by filtration, washed with water, and dried. Purification was carried out through a short column of alumina (dimensions 15 × 2 cm) in acetone. The product was precipitated from acetone/water, collected by filtration, washed with chilled water, and dried to afford a yellow solid. Yield: 110 mg, 48%. Anal. Calcd for C$_{66}$H$_{68}$Cl$_2$F$_{12}$N$_{14}$P$_2$O$_4$Ru$_3$·CH$_3$COCH$_3$: C,

45.0; H, 4.1; N, 10.6. Found: C, 44.9; H, 4.9; N, 10.2. ^{1}H NMR (CD$_3$COCD$_3$, δ_H/ppm): 8.40 (16H, d, H$^{2,6}_{py}$ × 8), 8.07 (8H, d, H$^{2,6}_{MeOpy}$ × 8), 7.87 (8H, t, H$^4_{py}$ × 8), 7.15 (16H, t, H$^{3,5}_{py}$ × 8), 6.62 (8H, d, H$^{3,5}_{MeOpy}$ × 4), 3.91 (12H, s, OCH$_3$ × 4). IR (KBr): ν(CN) 2068 (s) cm^{-1}.

Physical Measurements. IR spectra were collected as KBr pellets or acetonitrile solutions with a Nicolet FTIR 510P instrument. UV−visible spectra were recorded with a Hewlett-Packard 8453 diode-array spectrometer (range 190−1100 nm) or with a Shimadzu 3100 UV−visible−near-IR (NIR) spectrometer for wavelengths up to 2700 nm. NMR spectra were measured with a Bruker ARX500 spectrometer, using deuterated solvents from Aldrich. Elemental analyses were performed with a Carlo Erba 1108 analyzer. Cyclic voltammetry measurements were performed under argon with millimolar solutions of the compounds, using a TEQ V3 potentiostat and a standard three-electrode arrangement consisting of a glassy carbon disk (area = 9.4 mm^2) as the working electrode, a platinum wire as the counter electrode, and a silver wire as the reference electrode plus an internal ferrocene (Fc) or decamethylferrocene (Me$_{10}$Fc) standard.[18] [TBA]-PF$_6$ (0.1 M) was used as the supporting electrolyte in acetonitrile. All of the potentials reported in this work are referenced to the standard Ag/AgCl-saturated KCl electrode (0.197 V vs NHE), with the conversions being performed with literature values for the Fc$^+$/Fc or Me$_{10}$Fc$^+$/Me$_{10}$Fc couple in different media.[18] All of the spectroelectrochemical (SEC) experiments were performed using a three-electrode optically transparent thin-layer electrode cell.[19]

X-ray Structure Determinations. Suitable crystals of [**1**]PF$_6$, **2**, and [**4**](PF$_6$)$_2$ were grown by the slow diffusion of diethyl ether vapor into acetonitrile solutions of the compounds at −18 °C. Crystals were coated with perfluoropolyether, picked up with nylon loops, and mounted in an Oxford Xcalibur, Eos, Gemini CCD area-detector diffractometer using graphite-monochromated Mo Kα radiation (λ = 0.71069 Å) at 298 K. Final cell constants were obtained from least-squares fits of several thousand strong reflections. Data were corrected for absorption with *CrysAlisPro*, version 1.171.33.66 (Oxford Diffraction Ltd.), applying an empirical absorption correction using spherical harmonics, implemented in the *SCALE3 ABSPACK* scaling algorithm.[20] The structures were solved by direct methods with *SHELXS-97*[21] and refined by full-matrix least squares on F^2 with *SHELXL-97*.[21] All non-hydrogen atoms were refined anisotropically, and hydrogen atoms bound to carbon were placed at calculated positions and refined as riding atoms with isotropic displacement parameters. In compound [**1**]PF$_6$, the solvent molecules are disordered and could not be modeled properly. Therefore, the program *SQUEEZE*, a part of the *PLATON* package of crystallographic software,[22] was used to calculate the solvent disorder area and remove its contribution to the overall intensity data. In the case of compound [**4**](PF$_6$)$_2$, because of moderate crystal quality, similarity restraints were applied to the bridging carbon and nitrogen atoms to prevent anisotropic refinement bumping. Final crystallographic data and the values of R1 and wR2 are listed in Table S1 in the Supporting

Table 1. Selected Bond Distances and Angles for the Cation in [1]PF$_6$, Complex 2, and the Cation in [4](PF$_6$)$_2$

					[4](PF$_6$)$_2$	
	[1]PF$_6$			2	Ru$_{central}$	Ru$_{terminal}$
			Distances/Å			
Ru–Cl	**Ru–Cl**	**Ru–Cl**	**Ru–CN**	**Ru–CN**	**Ru–CN**	**Ru–NC**
2.3941(11)	2.3960(11)	2.3986(11)	2.036(6)	2.043(7)	1.99(3)	2.07(2)
			2.036(6)	2.062(7)	2.11(2)	2.020(16)
Ru–NCMe	**Ru–NCMe**	**Ru–NCMe**	**RuC–N**	**RuC–N**	**RuC–N**	**Ru–Cl**
2.002(3)	2.001(3)	1.997(3)	1.160(7)	1.134(8)	1.12(3)	2.385(6)
			1.153(6)	1.139(8)	1.05(2)	2.392(6)
Ru–N$_{py}$	**Ru–N$_{py}$**	**Ru–N$_{py}$**	**Ru–N$_{MeOpy}$**	**Ru–N$_{MeOpy}$**	**Ru–N$_{MeOpy}$**	**Ru–N$_{py}$**
2.076(3)	2.089(3)	2.079(3)	2.105(5)	2.097(4)	2.095(8)	2.066(12)
2.085(3)	2.091(3)	2.086(3)	2.114(4)	2.109(4)		2.068(12)
2.087(3)	2.094(3)	2.087(4)	2.116(5)	2.105(4)		
2.097(3)	2.099(3)	2.093(3)	2.103(4)	2.104(4)		
RuN–CMe	**RuN–CMe**	**RuN–CMe**				
1.152(4)	1.143(5)	1.130(5)				
			Angles/deg			
Cl–Ru–NCMe	**Cl–Ru–NCMe**	**Cl–Ru–NCMe**	**Ru–C–N**	**Ru–C–N**	**Ru–C–N**	**Ru–N–C**
179.37(10)	179.26(10)	178.29(9)	178.6(5)	176.6(6)	180.000(2)	180.000(1)
			174.8(6)	176.7(5)	180.0	180.000(2)
Ru–N–CMe	**Ru–N–CMe**	**Ru–N–CMe**	**NC–Ru–CN**	**NC–Ru–CN**	**NC–Ru–CN**	**CN–Ru–Cl**
176.0(3)	174.6(3)	173.9(3)	177.7(2)	179.1(2)	180.000(1)	180.000(1)
						180.0
N–C–Me	**N–C–Me**	**N–C–Me**				
178.6(5)	177.5(5)	178.3(5)				
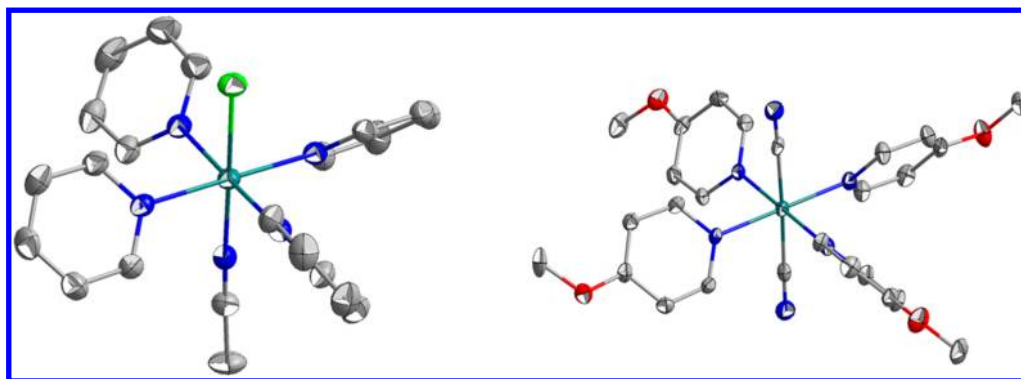
Figure 1. Structural representations of one of the independent complex cations in [1]PF$_6$ (left) and 2 (right), with hydrogen atoms omitted for the sake of clarity. The thermal ellipsoids correspond to 30% probability.
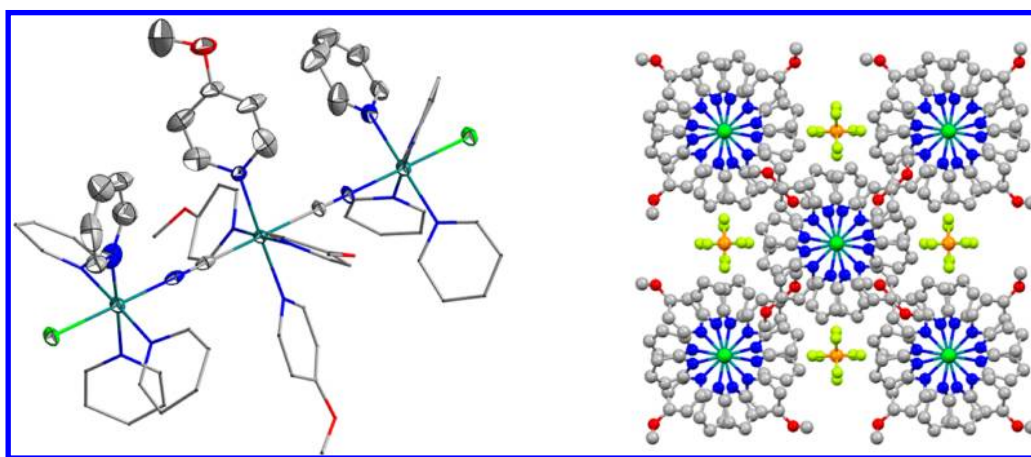
Figure 2. Structural representation of the complex cation in [4](PF$_6$)$_2$ (left) and crystal packing of [4](PF$_6$)$_2$ (right) viewed along the Cl–Ru–NC–Ru–CN–Ru–Cl axis showing the staggered configuration of the coordination spheres of the metal ions. The hydrogen atoms are omitted for the sake of clarity, and the thermal ellipsoids correspond to 30% probability.

Information, while the main angles and distances are listed in Table 1. CCDC 895589−895591 contain the supplementary crystallographic data for this paper. These data can be obtained free of charge from the Cambridge Crystallographic Data Center via www.ccdc.cam.ac.uk/data_request/cif.

■ RESULTS

Crystallography. Figure 1 shows the molecular structures of the monometallic complexes in [**1**]PF$_6$ and **2**. The crystal structure of [**1**]PF$_6$ contains three independent cations with very similar geometric parameters (Table 1) and two molecules of methanol in the asymmetric unit. All three cations show the characteristic propeller-like arrangement of the *trans*-tetrapyridine fragment, arising from a tilting of the pyridine rings with respect to the RuN$_4$ plane in order to reduce mutual repulsions. The range of the Ru−N$_{py}$ distance [2.076(3)−2.099(3) Å] is similar to those found in related complexes.[14] The range of the Ru−NCMe distance [1.997(3)−2.002(3) Å] is considerably shorter, suggesting extensive dπ(Ru^{II}) → π* back-bonding to the acetonitrile ligand and a stronger metal−nitrogen bond. The Cl−Ru−NCMe unit is approximately linearly bound, with Cl−Ru−N, Ru−N−C, and N−C−Me bond angles of 178.29(9)−179.37(10), 173.9(3)−176.0(3), and 177.5(5)−178.6(5)°, respectively. The range of the Ru−Cl bond distance of 2.3941(11)−2.3986(11) Å is very similar to that found in *trans*-[Ru^{II}Cl(py)$_4$(PhCN)]PF$_6$.[14]

The asymmetric unit of the structure of **2** (Figure 1) contains two independent molecules and no solvent ones. Both molecules also show the typical propeller disposition of the MeOpy ligands and a linear arrangement of the *trans*-{Ru^{II}(CN)$_2$} motif, similar to that observed in the acetonitrile solvate of the related complex **5**.[11] The range of the Ru−N distance in **2** is slightly longer than that found in **5**·2MeCN [2.097(4)−2.116(5) vs 2.091(4) Å], while the range of the Ru−C distance is similar, [2.036(6)−2.062(7) vs 2.057(4) Å].

Figure 2 shows the crystal structure of the complex salt [**4**](PF$_6$)$_2$, which crystallized without any included solvent molecules. This cation shows a linear arrangement of the {Cl−Ru−NC−Ru−CN−Ru−Cl} unit similar to that observed in [**7**](PF$_6$)$_2$·5MeCN·py,[11] but the coordination spheres of the metal ions are staggered instead of eclipsed (see Figure 2). The distances involving the central ruthenium atom are remarkably similar to those observed in [**7**](PF$_6$)$_2$·5MeCN·py. For the terminal ruthenium atoms, the Ru−Cl distance is shorter in [**4**](PF$_6$)$_2$ [2.385(6)−2.392(6) vs 2.4312(24) Å], while the Ru−N(nitrile) distance is longer [2.020(16)−2.07(2) vs 2.013(8) Å].

Electrochemistry. Cyclic voltammograms in acetonitrile of [**3**]PF$_6$ and [**4**](PF$_6$)$_2$ are shown in Figure 3, while the relevant electrochemical data are presented in Table 2. All of the observed couples are electrochemically reversible and correspond to oxidation of the ruthenium centers.

The presence of the more basic ligands in complex **2** decreases the ruthenium(III/II) potential by 180 mV compared to that of **5**. Similar shifts are observed for the couples associated with oxidation of the moiety **2** in the polymetallic species [**3**]PF$_6$ and [**4**](PF$_6$)$_2$.

For the bimetallic complex in [**3**]PF$_6$, oxidation of the {Ru^{II}(py)$_4$Cl}$^+$ fragment occurs at almost the same potential as that observed for [**6**]PF$_6$. The same is true for the first oxidation of the trimetallic complexes in [**4**](PF$_6$)$_2$ and [**7**](PF$_6$)$_2$. Therefore, replacing py with MeOpy in the central ruthenium moiety has very little effect on the electronic
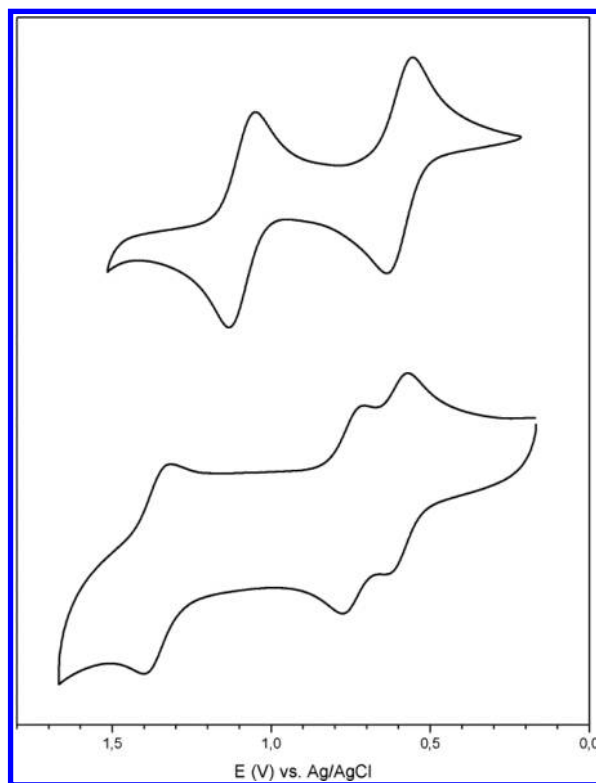

Figure 3. Cyclic voltammograms of [**3**]PF$_6$ (top) and [**4**](PF$_6$)$_2$ (bottom) in 0.1 M [TBA]PF$_6$ in acetonitrile at a 200 mV s^{-1} scan rate.

properties of the adjacent {Ru^{II}(py)$_4$Cl} units. The second Ru^{II}(py)$_4$Cl-based oxidation of [**4**](PF$_6$)$_2$ is observed at 0.75 V, 150 mV higher than the first oxidation potential. The corresponding $\Delta E_{1/2}$ value is larger than that of 100 mV observed for [**7**](PF$_6$)$_2$. The separation between the different redox processes of these complexes is large enough to allow for spectroscopic characterization of all of the different redox states (see below).

Electronic Spectroscopy. The absorption maxima data for all of the compounds considered in this work are listed in Table 3. All of them exhibit the electronic spectroscopic features expected for ruthenium(II) pyridine chromophores: sharp ligand-centered π → π* transitions in the UV region of the spectrum and intense broad bands in the visible region, corresponding to dπ(Ru^{II}) → π*(pyridine) metal-to-ligand charge-transfer (MLCT) transitions (see Figure S1 in the Supporting Information). The intensities of these bands are roughly proportional to the number of ruthenium units present.

SEC measurements have been carried out for the oxidized forms of these multimetallic complexes, and the resulting data are included in Table 3. Figure 4 shows the effects of one-electron oxidation of the bimetallic complexes **6**$^+$ and **3**$^+$. The main new feature is a strong band in the NIR region, which is centered at 8400 cm^{-1} for **6**$^{2+}$ and shifted to lower energy in **3**$^{2+}$ (7200 cm^{-1}). In the latter case, this band is relatively more intense (ε = 8500 and 6000 M^{-1} cm^{-1} for **3**$^{2+}$ and **6**$^{2+}$, respectively) and asymmetrical with a half-bandwidth on the low-energy side narrower than that on the high-energy side. A weak shoulder at around 4200 cm^{-1} can also be distinguished (Figure S2 in the Supporting Information). These stretches are characteristic of the mixed-valence forms of these bimetallic complexes because they disappear upon further oxidation and

Table 2. Electrochemical Data in Acetonitrile: $E_{1/2}[\mathrm{Ru^{III/II}}]$/V vs Ag/AgCl (KCl ss) ($\Delta E_p$/mV)

complex	L	RuL$_4$(CN)$_2$[a]	Ru(py)$_4$Cl[b]	Ru(py)$_4$Cl[b']	ΔE_{a-b}	$\Delta E_{b-b'}$
2	MeOpy	0.67 (70)				
3$^+$	MeOpy	1.08 (70)		0.59 (70)	0.49	
4^{2+}	MeOpy	1.36 (70)	0.75 (70)	0.60 (70)	0.61	0.15
5	py	0.85 (70)				
6$^+$	py	1.25 (70)		0.58 (70)	0.67	
7^{2+}	py	1.56 (75)	0.69 (70)	0.59 (75)	0.87	0.10

Table 3. UV−Visible and NIR Absorption Data in Acetonitrile

complex	L	MLCT^a ν_{max}/cm^{-1} (ε/M^{-1} cm^{-1})	MM′CT^b ν_{max}/cm^{-1} (ε/M^{-1} cm^{-1}) [$\Delta\nu$/ cm^{-1}]	MMCT^b ν_{max}/cm^{-1} (ε/M^{-1} cm^{-1}) [$\Delta\nu$/ cm^{-1}]
1$^+$	py	28200 (22200)		
2	MeOpy	28400 (20500)		
3$^+$	MeOpy	27500 (34300)		
3^{2+}	MeOpy	31700 (23900)	7200 (8500) [3100]	
4^{2+}	MeOpy	27400 (46900)		
4^{3+}	MeOpy	28600 (27600)^c	9400sh (2200) [3500]^{c,d}	5600 (6100) [4400]^{c,d}
4^{4+}	MeOpy	33300sh (27600)	9100 (10000) [3400]	
5	py	26700 (22500)		
6$^+$	py	26700 (42600)		
6^{2+}	py	30100 (20500)	8400 (6000) [3400]	
7^{2+}	py	27100 (51800)		
7^{3+}	py	27900 (29000)^c	10600 (2000) [3800]^{c,d}	5900 (5200) [4100]^{c,d}
7^{4+}	py	31700sh (19500)	10500 (9300) [3100]	

^{a}For the spectra, see Figure S1 in the Supporting Information. ^{b}MM′CT corresponds to a transition between metal ions with different coordination spheres, while MMCT indicates a transition between ions with identical coordination spheres. ^{c}Corrected for comproportionation. ^{d}Spectral parameters obtained by Gaussian deconvolution with spectral fitting procedures (see Figure S3 in the Supporting Information).

are attributable to MM′CT between the two distinct ruthenium centers.

The fully oxidized forms of the bimetallic complexes are characterized by a series of bands in the visible region, probably ligand-to-metal charge transfer (LMCT) in character. These bands resemble those observed for the ruthenium(III) forms of the monometallic species (Table 4 and Figure S4 in the Supporting Information).

The spectra of the one-electron-oxidized forms of the trinuclear complexes show two bands in the NIR region (Figure 5), instead of a single one, attributable to MMCT transitions due to the presence of two different ruthenium(II) donors and one ruthenium(III) acceptor. For **7**$^{3+}$, the two bands are well-resolved at 10600 and 5900 cm^{-1}, with the latter being more intense. In contrast, the spectrum of **4**$^{3+}$ shows two severely overlapped bands at ca. 9400 and 5600 cm^{-1}. Upon oxidation by one more electron, both complexes behave similarly; the band to low energy disappears, and the other gains intensity and shifts slightly to the red. The full three-electron oxidation of the trimetallic complexes results in the disappearance of the intense NIR band, which is replaced by a set of bands to higher energies that resemble those observed for the ruthenium(III) forms of the mono- and bimetallic complexes (Table 4 and Figure S4 in the Supporting Information).

IR Spectroscopy. All of the complexes considered here exhibit bands between 2200 and 2000 cm^{-1} assigned to ν(CN) stretches (Table 5). In their reduced forms, all of them show bands between 2068 and 2060 cm^{-1}, which are typical of ruthenium(II) cyano compounds.[23,24] Coordination of the {Ru^{II}(py)$_4$Cl}$^+$ moieties results in decreased intensities for the ν(CN) bands as the change in the dipole moment associated with the stretching vibration is diminished.[11]

One-electron oxidation of the bimetallic complexes (Figure 6) results in the development of a new very strong band shifted to lower energies (2004 cm^{-1} for **6**$^{2+}$ and 1993 cm^{-1} for **3**$^{2+}$) and a less intense band shifted to higher frequencies (2099 cm^{-1} for **6**$^{2+}$ and 2098 cm^{-1} for **3**$^{2+}$). Further oxidation of the complexes results in the disappearance of the strong bands and their replacement by signals around 2100 cm^{-1}, as expected for ruthenium(III) cyano compounds.[25,26]

Oxidation by one electron of the trimetallic complexes (Figure 7) shows a pattern similar to that observed for their dinuclear counterparts; a very strong band shifted to lower energies (2018 cm^{-1} for **7**$^{3+}$ and 2008 cm^{-1} for **4**$^{3+}$) and a less intense band at higher energies (2080 cm^{-1} for **7**$^{3+}$ and 2077 cm^{-1} for **4**$^{3+}$). Also, a broad band centered around 1950 cm^{-1} is observed that is probably electronic in character (see the Discussion section). Upon further one-electron oxidation, the intensity of the band around 2000 cm^{-1} is enhanced, while the other two bands vanish. Finally, the spectra of the fully oxidized species show only a broad band around 2100 cm^{-1}.

■ DISCUSSION

The evidence available in the literature supports the ability of the cyanide bridge to promote electronic coupling between metal ions, which results in a class II behavior.[1,3,5,15,27−32] However, none of the cyanide-bridged systems reported so far can be described as class III (i.e., valence-delocalized). This is most probably due to the energy differences in the metal orbitals introduced by the asymmetry of the cyanide bridge, with the carbon end stabilizing the low-valent donor site. Nevertheless, this effect can be mitigated by tuning the electronic properties of the metallic fragments via their auxiliary ligands. For example, recently we have reported a system where the asymmetry of the bridge was compensated for by the
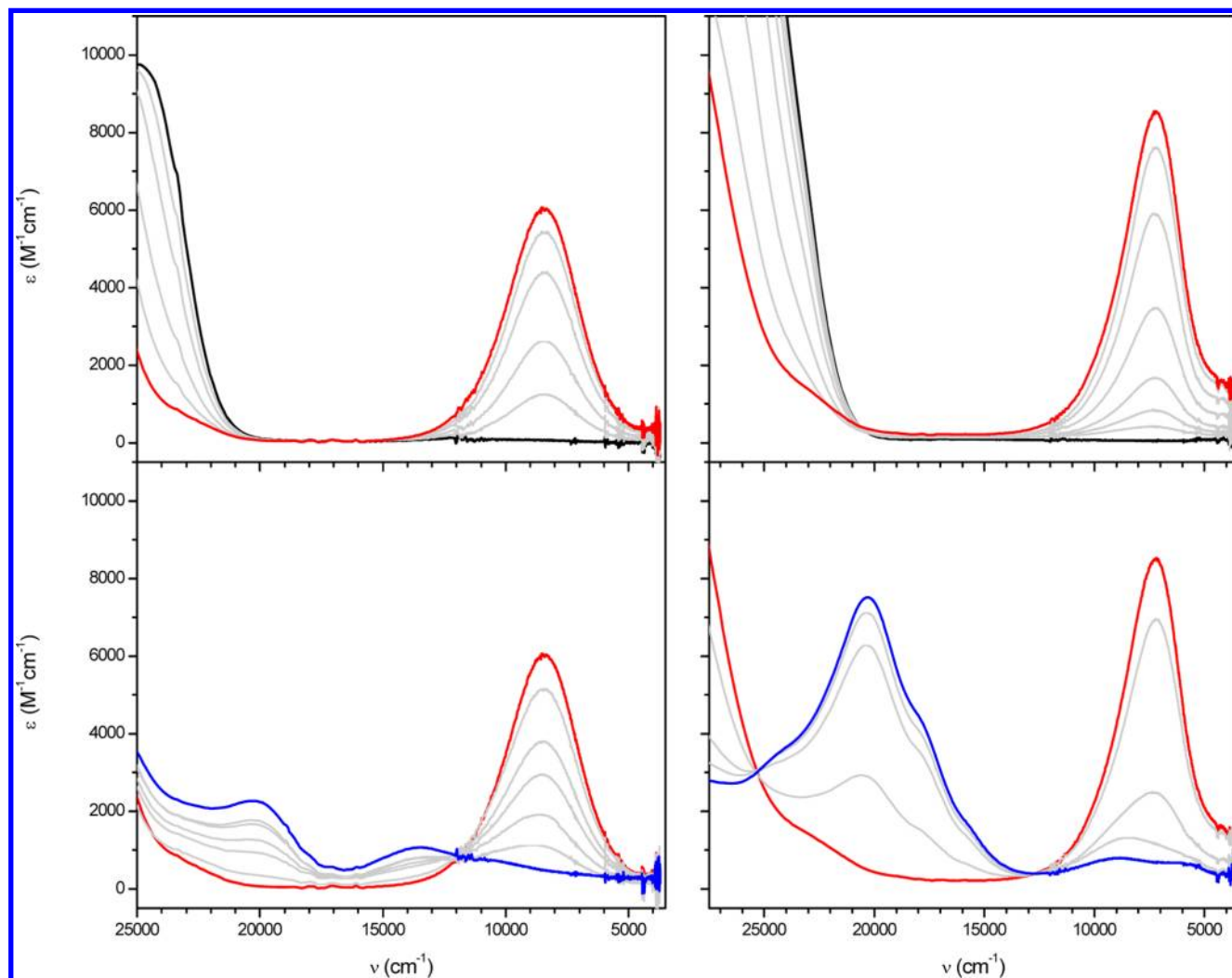
2910

dx.doi.org/10.1021/ic302173g | Inorg. Chem. 2013, 52, 2906−2917

Figure 4. Vis−NIR spectroelectrochemistry for [**6**]PF$_6$ (left) and [**3**]PF$_6$ (right). Top: first oxidation process. Bottom: second oxidation process. Formal ruthenium oxidation states: [II, II] black lines; [III, II] red lines; [III, III] blue lines.

different nature of the metal centers involved. In this system, the structural and spectroscopic evidence indicates such a degree of charge delocalization that the metals are better described as having partial redox states.[33]

Following this approach, we have prepared the bimetallic complex **3**$^+$ and the trimetallic complex **4**$^{2+}$ containing the relatively electron-rich MeOpy ligand. Here we aim to lower the ruthenium(III/II) redox potential of the dicyano fragment to make it closer to that of the terminal {Ru^{II}(py)$_4$Cl}$^+$ units compared to the system previously reported by Coe et al.[11]

The electrochemistry results found for the new complexes prove our approach to be successful. Introducing MeOpy in place of py ligands lowers the ruthenium(III/II) redox potential of *trans*-[Ru^{II}(CN)$_2$L$_4$] fragments by 170−200 mV (Table 2). This structural modification also increases the ruthenium(III/II) potential splitting of the terminal Ru^{II}(py)$_4$Cl fragments in the trimetallic complex **4**$^{2+}$ (Figure 3), indicating an increased electronic mixing between the metal sites.[12]

The previously reported X-ray crystal structure of **7**$^{2+}$ as its hexafluorophosphate salt shows an eclipsed configuration of the three metal coordination spheres, and it was suggested that this arrangement might facilitate electronic coupling between the ruthenium centers.[11] However, the structure of the closely related **4**$^{2+}$ (Figure 2) reveals a staggered configuration. Clearly,

any electronic factors that may favor an eclipsed geometry are overridden by crystal packing forces. The packing interactions probably mask any possible difference in the geometric data between these trimetallic complexes.

The NIR spectra of the mixed-valence form of the bimetallic (**3**$^{2+}$ and **6**$^{2+}$) and trimetallic (**4**$^{3+}$ and **7**$^{3+}$) complexes are very informative regarding intermetallic electronic communication. Relevant data are summarized in Table 6. The intense NIR bands of the bimetallic species show a shift to lower energies of 1200 cm^{-1} on moving from **6**$^{2+}$ to **3**$^{2+}$ (Figure 4). This shift is in agreement with a MM′CT assignment because the donating ruthenium(II) center is more electron-rich when coordinated to MeOpy rather than py ligands. A Mulliken−Hush analysis[34−36] of this band affords H_{ab} values of 1700 and 1800 cm^{-1} for **6**$^{2+}$ and **3**$^{2+}$, respectively, in accordance with the values obtained for other cyanide-bridged diruthenium complexes.[24,37−42] These values indicate significant orbital mixing between the donor−acceptor metal sites, as represented by the derived α^2 values, which measure the extent of electronic delocalization,[2] of 4% for **6**$^{2+}$ and 7% for **3**$^{2+}$ (Table 6). These values are probably seriously underestimated because the previous calculation overestimates the effective dipole length in systems with considerable mixing.[43,44] The NIR band in **3**$^{2+}$

Table 4. UV−Visible Data in Acetonitrile for the Fully Oxidized Ruthenium(III) Species[a]

complex	L	LMCT ν_{max}/cm^{-1} ($\varepsilon/M^{-1}\,cm^{-1}$)	assignment
1^{2+}	py	26800sh (1100)	$\pi(py) \rightarrow d\pi(Ru^{III})$
		24300 (1400)	$\pi(py) \rightarrow d\pi(Ru^{III})$
		21300sh (400)	$\pi(Cl) \rightarrow d\pi(Ru^{III})$
2^{+}	MeOpy	25000sh (2500)	$\pi(MeOpy) \rightarrow d\pi(Ru^{III})$
		22200 (8600)	$\pi(MeOpy) \rightarrow d\pi(Ru^{III})$
		19800sh (3000)	$\pi(MeOpy) \rightarrow d\pi(Ru^{III})$
3^{3+}	MeOpy	24200sh (2500)	$\pi(MeOpy) \rightarrow d\pi(Ru^{III})$
		20100 (7400)	$\pi(MeOpy) \rightarrow d\pi(Ru^{III})$
		17900sh (4600)	$\pi(MeOpy) \rightarrow d\pi(Ru^{III})$
4^{5+}	MeOpy	24400sh (4300)	$\pi(MeOpy) \rightarrow d\pi(Ru^{III})$
		18700 (9200)	$\pi(MeOpy) \rightarrow d\pi(Ru^{III})$
		16100sh (3300)	$\pi(MeOpy) \rightarrow d\pi(Ru^{III})$
5^{+}	py	26300 (2100)	$\pi(py) \rightarrow d\pi(Ru^{III})$
		21300 (700)	$\pi(py) \rightarrow d\pi(Ru^{III})$
6^{3+}	py	25300 (4200)	$\pi(py) \rightarrow d\pi(Ru^{III})$
		20000 (2200)	$\pi(py) \rightarrow d\pi(Ru^{III})$
		13300 (600)	$\pi(Cl) \rightarrow d\pi(Ru^{III})$
7^{5+}	py	25000 (6500)	$\pi(py) \rightarrow d\pi(Ru^{III})$
		21500sh (4000)	$\pi(py) \rightarrow d\pi(Ru^{III})$
		11000 (1100)	$\pi(Cl) \rightarrow d\pi(Ru^{III})$

[a]For the spectra, see Figure S4 in the Supporting Information.

is clearly asymmetric, which may be due to multiple transitions involving different ruthenium(II) $d\pi$ donor orbitals.[45]

The two NIR bands observed for the one-electron-oxidized forms of the trimetallic complexes **7**$^{3+}$ and **4**$^{3+}$ (Figure 5) correspond to a charge transfer from the central ruthenium(II) unit to the neighboring terminal Ru^{III}(py)$_4$Cl fragment (MM′CT) and a charge transfer between the distant Ru(py)$_4$Cl fragments (MMCT), but their assignment is not straightforward. The less intense, higher-energy NIR band shifts to the red upon replacement of the py ligands (**7**$^{3+}$) by MeOpy (**4**$^{3+}$). This effect suggests significant participation of the Ru^{II}L$_4$(CN)$_2$ fragment, which becomes more electron-rich as MeOpy replaces py, so we assign this band as MM′CT. Moreover, the corresponding shift in energy (ca. 1200 cm^{-1}) is essentially identical with that observed on moving from the bimetallic complex **6**$^{2+}$ to **3**$^{2+}$. Therefore, the other band at lower energy for **7**$^{3+}$ and **4**$^{3+}$ corresponds to MMCT, mostly unaffected by the ligand replacement at the central ruthenium moiety. This band disappears upon two-electron oxidation, supporting our assignments. However, these assignments may correspond with an incomplete description of the system because substantial mixing between the excited states may be operative. The fact that the energies of the MM′CT transitions in the bimetallic complexes **3**$^{2+}$ and **6**$^{2+}$ are both nearly averages of those of the MMCT and MM′CT transitions in the corresponding trimetallic complexes is indicative of the mixing of configurations.

Several observations of MMCT transitions between next-to-nearest-neighbor ruthenium centers in trimetallic complexes have been reported previously,[37,38,42,46] but in those examples, these transitions are less intense than the MM′CT ones. For the cyanide-bridged Ru$_4$ square,[47] where the difference in the chemical environment and thus energy between the metal centers are smaller, the NIR absorption profiles resemble those reported here. In this case, the two observed NIR bands have also been assigned as mixtures of the MMCT and MM′CT transitions.[47]

In these systems, a simple two-state model is not fully applicable but can be used as an approximation. Application of the Hush formalism[34,35] to the deconvoluted bands results in H_{ab} (α^2) values for the MMCT transition of 800 cm^{-1} (1.9%) for **4**$^{3+}$ and 700 cm^{-1} (1.4%) for **7**$^{3+}$ (Table 6). These values indicate a substantial interaction between the $d\pi$ orbitals of the terminal ruthenium ions, similar to that observed for other localized class II mixed-valence complexes.[48] It is worth mentioning that the interaction is slightly, but clearly, more pronounced in **4**$^{3+}$, indicating that bringing the HOMO energy of the central ruthenium closer to that of the terminal ones increases the mixing between the $d\pi$ orbitals of the three metal ions.

For the vicinal MM′CT transition, the Hush parameters are 1100 cm^{-1} (1.3%) for **4**$^{3+}$ and 1100 cm^{-1} (1.1%) for **7**$^{3+}$, lower than those for the binuclear systems and consistent with the electron density being distributed over one more ruthenium center.

Two-electron oxidations of the trinuclear complexes give **7**$^{4+}$ and **4**$^{4+}$, with formal configurations [III, II, III]. As expected, the lower-energy MMCT band disappears and the intensity of the higher-energy MM′CT band increases (Figure 5) because the transition includes now two acceptor terminal ruthenium-(III) units. The Hush parameters H_{ab} and α^2 for **7**$^{4+}$ and **4**$^{4+}$ (Table 6) are similar to those for the binuclear systems, indicating a substantial mixing between the $d\pi$ orbitals of the vicinal ruthenium atoms, but still compatible with a valence-localized description.

The IR spectra of the bimetallic complexes (Figure 6) are also very informative. The $\nu(CN)$ band of a bridging cyanide can be shifted significantly to lower energies and intensified in the presence of a strong donor−acceptor interaction,[24,27,28,31,39,42,49,50] attributable to vibronic coupling with a MM′CT transition.[42] Hence, we assign the very strong band at 2004 cm^{-1} for **6**$^{2+}$ to the bridging cyanide, while that at 2099 cm^{-1} corresponds to the terminal one. The slightly lower $\nu(CN)$ energy observed for **3**$^{2+}$ (1993 cm^{-1}) probably arises from the relatively higher degree of intermetallic electronic
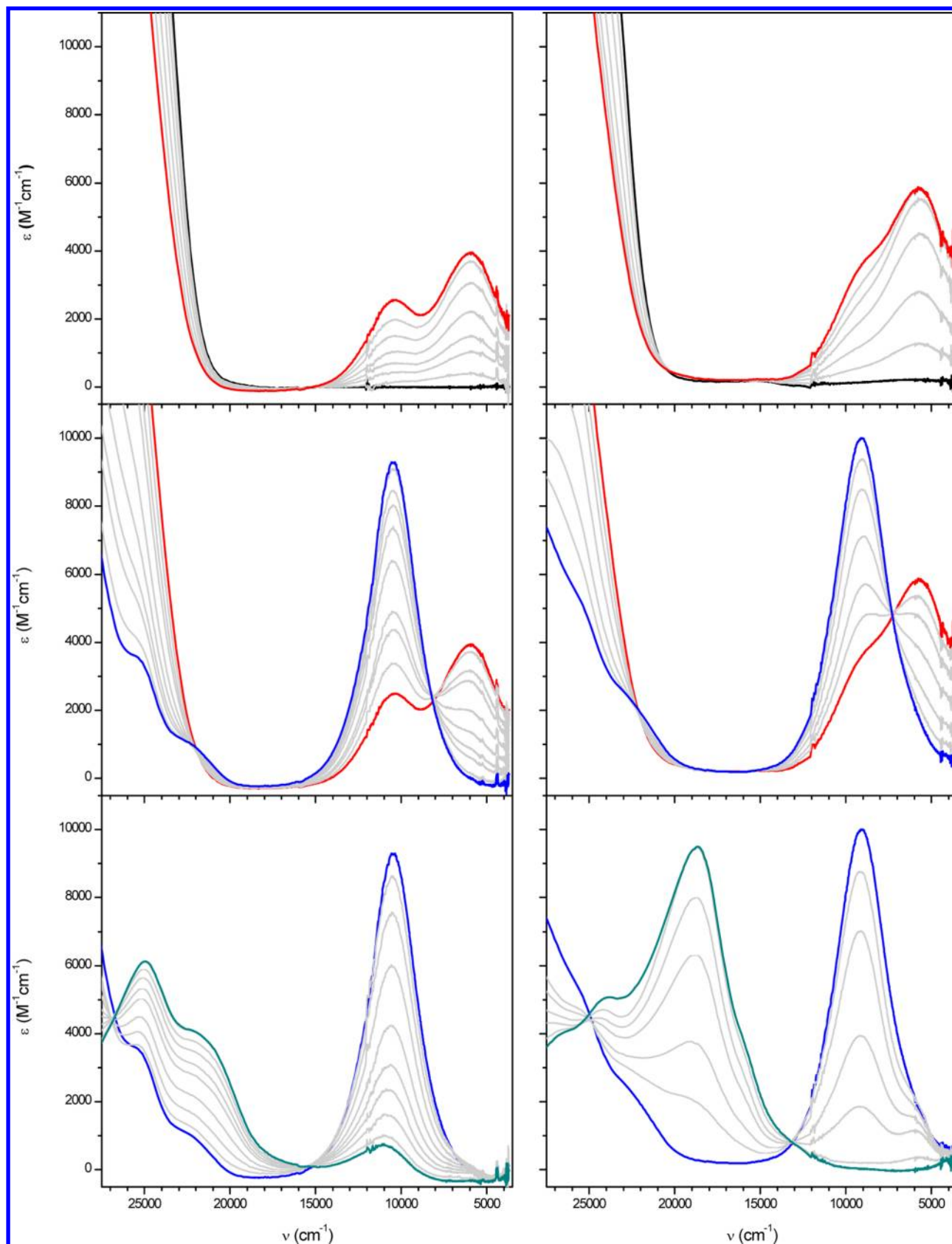
Figure 5. Vis−NIR spectroelectrochemistry for $[7](PF_6)_2$ (left) and $[4](PF_6)_2$ (right). Top: first oxidation process. Middle: second oxidation process. Bottom: third oxidation process. Formal ruthenium oxidation states: [II, II, II] black lines; [III, II, II] red lines; [III, II, III] blue lines; [III, III, III] dark cyan lines.

Table 5. IR Data in Acetonitrile

complex	L	formal oxidation states	$\nu(CN)/cm^{-1}$
2	MeOpy	[II]	2060(s)
2+	MeOpy	[III]	2112
3+	MeOpy	[II, II]	2083, 2057(s)
32+	MeOpy	[III, II]	2098, 1993(vs)
33+	MeOpy	[III, III]	2109sh, 2094
42+	MeOpy	[II, II, II]	2064(s)
43+	MeOpy	[III, II, II]	2077(s), 2008(vs)
44+	MeOpy	[III, II, III]	2008(vs)
45+	MeOpy	[III, III, III]	2103
5	py	[II]	2062
5+	py	[III]	2108
6+	py	[II, II]	2087, 2064(s)
62+	py	[III, II]	2099, 2004(vs)
63+	py	[III, III]	2109, 2089
72+	py	[II, II, II]	2068(s)
73+	py	[III, II, II]	2080(s), 2018(vs)
74+	py	[III, II, III]	2018(vs)
75+	py	[III, III, III]	2112

coupling, as shown by the electrochemical and electronic absorption data.

The IR spectra of $\mathbf{4}^{3+}$ and $\mathbf{7}^{3+}$ show two distinct $\nu(CN)$ bands (Figure 7), confirming that an asymmetric localized [III, II, II] description is appropriate for these systems. One band is very intense and displaced to lower energies, while the other is slightly shifted to higher energies compared with that of the reduced form. The energy and intensity of the former resemble the behavior of the $\nu(CN)$ band in the mixed-valence forms of the bimetallic complexes, so we assign it to the bridge connecting ruthenium(II) and ruthenium(III). Supporting the previous assignment, the spectra of the two-electron-oxidized complexes $\mathbf{4}^{4+}$ and $\mathbf{7}^{4+}$ show only one very strong $\nu(CN)$ band at 2008 and 2018 cm^{-1}, respectively, as expected for a [III, II, III] configuration with two symmetry-related bridging cyanides connecting ruthenium(II) to ruthenium(III).

The band centered around 1950 cm^{-1} for $\mathbf{4}^{3+}$ and $\mathbf{7}^{3+}$ is absent in the other redox forms of the trinuclear complexes and is too broad to be vibronic in origin ($\Delta\bar{\nu} = 150$ cm^{-1}). Hence, we assume this band to be an electronic transition. We should rule out a dominant MM′CT character because that is incompatible with its width and energy. A more feasible origin is an intraconfigurational transition between the ruthenium d−d states split by spin−orbit coupling. Such spin-forbidden transitions are not observed usually in ruthenium(III) complexes, but have been reported as weak narrow bands around 5000 cm^{-1} for osmium(III) complexes. Interestingly, in
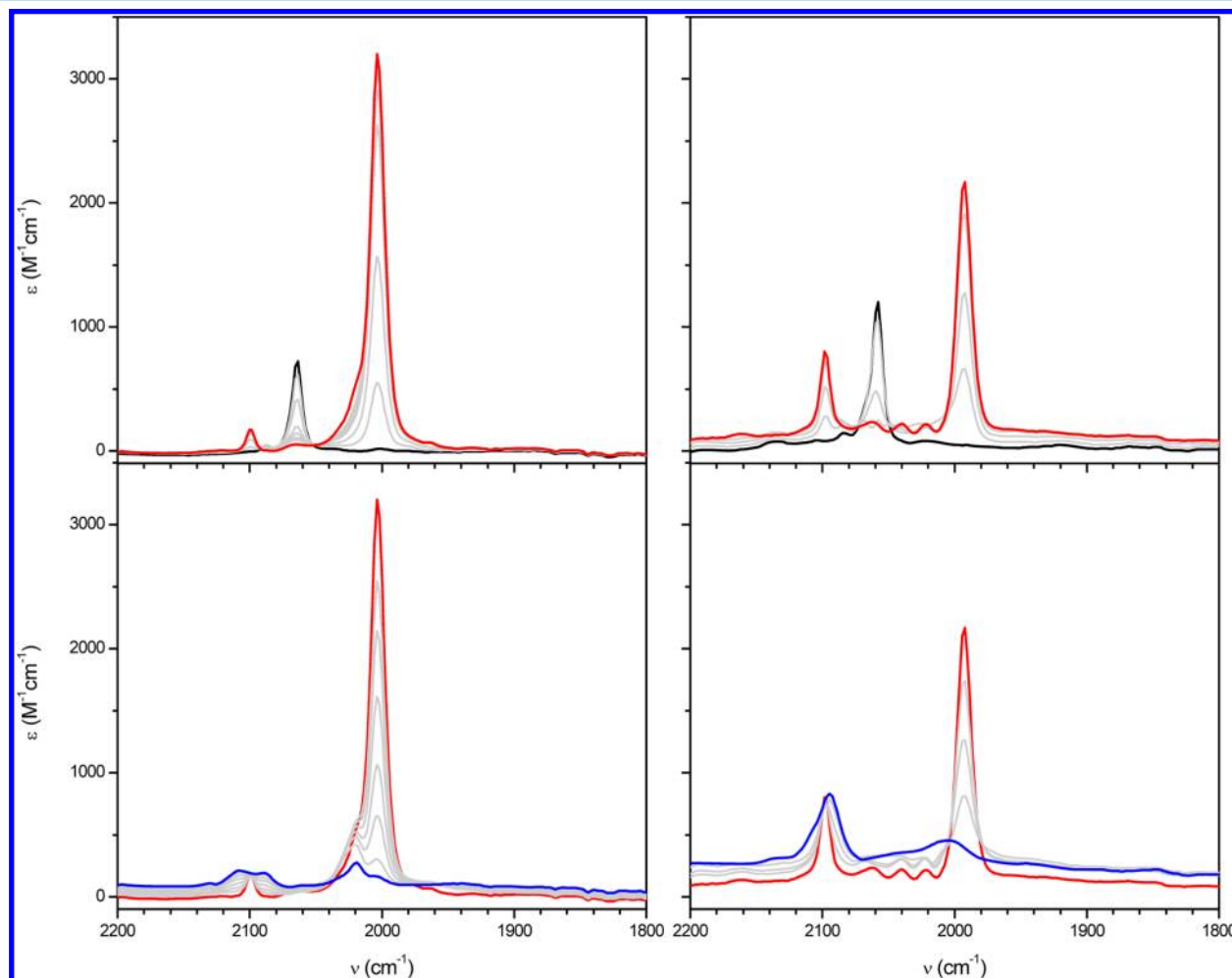

Figure 6. IR spectroelectrochemistry for [**6**]PF$_6$ (left) and [**3**]PF$_6$ (right). Top: first oxidation process. Bottom: second oxidation process. Formal ruthenium oxidation states: [II, II] black lines; [III, II] red lines; [III, III] blue lines.
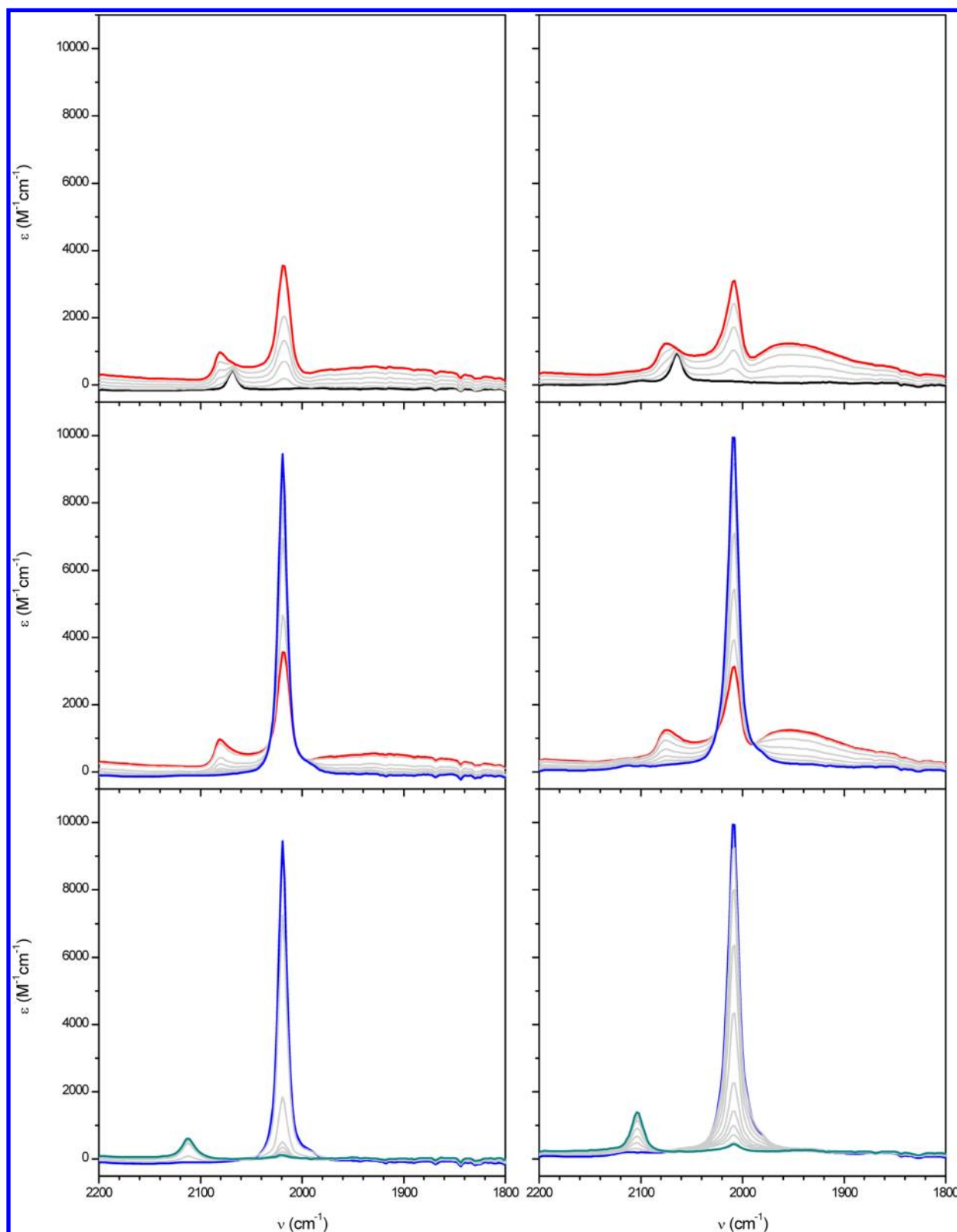
Figure 7. IR spectroelectrochemistry for $[7](PF_6)_2$ (left) and $[4](PF_6)_2$ (right). Top: first oxidation process. Middle: second oxidation process. Bottom: third oxidation process. Formal ruthenium oxidation states: [II, II, II] black lines; [III, II, II] red lines; [III, II, III] blue lines; [III, III, III] dark cyan lines.

some mixed-valence osmium complexes,[13,33,51] these bands show an intensity enhancement and it has been proposed that mixing with a MMCT state is responsible for this effect. For a ruthenium complex, this transition would be expected at $\bar{\nu} \sim$

1500 cm^{-1} ($\bar{\nu} = {}^3/_2\xi$ with $\xi_{Ru} \sim 1000$ cm^{-1}).[52] The transition-observed energy is higher than this value, but a shift in energy may also arise if mixing with a MM′CT state is operative for these complexes.

2915

dx.doi.org/10.1021/ic302173g | *Inorg. Chem.* 2013, 52, 2906−2917

Table 6. Spectral Parameters for NIR Bands of Mixed-Valence Complexes in Acetonitrile[a]

complex	L	ν_{max}/cm^{-1} $(\varepsilon/M^{-1}\,cm^{-1})$ $[\Delta\nu/cm^{-1}]$	$\int\varepsilon(\nu)d\nu/10^6\,M^{-1}\,cm^{-2}$	r_{ab}/Å	α^2	H_{ab}/cm^{-1}
		Bimetallic Complexes				
3^{2+}	MeOpy	7200 (8500) [3100]	31.653[b]	5.18	0.066	1800
6^{2+}	py	8400 (6000) [3400]	22.423[b]	5.21	0.039	1700
		Trimetallic Complexes				
4^{3+}	MeOpy	9400 (2200) [3500][c]	8.201[d]	5.18	0.013	1100
		5600 (6100) [4400][c]	28.585[d]	10.37	0.019	800
4^{4+}	MeOpy	9100 (10000) [3400]	39.137[b]	5.18	0.032	1600
7^{3+}	py	10600 (2000) [3800][c]	8.094[d]	5.21	0.011	1100
		5900 (5200) [4100][c]	22.706[d]	10.42	0.014	700
7^{4+}	py	10500 (9300) [3100]	33.018[b]	5.21	0.023	1600

[a]$H_{ab} = \alpha\nu_{max}$ and $\alpha^2 = 4.0 \times 10^{-4}\int\varepsilon(\nu)d\nu/G\nu_{max}\,r_{ab}^2$ (2) with the degeneracy $G = 2$ for 4^{4+} and 7^{4+} and $G = 1$ for the rest. [b]Calculated by numerical integration of the experimental spectra. [c]Corrected for comproportionation. [d]Calculated as $\int\varepsilon(\nu)d\nu = [\pi/(4\ln2)]\varepsilon_{max}\Delta\nu_{1/2}$; the spectral parameters were obtained by Gaussian deconvolution of the experimental spectra (see Figure S3 in the Supporting Information).

All of the ruthenium(III) species show a variety of bands in the visible region of the spectrum that we assign to LMCT transitions (Table 4 and Figure S4 in the Supporting Information). The complexes bearing a MeOpy ligand show a more intense set of bands around 20000 cm⁻¹ that have their origin in the nπ orbitals of the methoxy substituent. The position of these bands shifts to the red on moving from the monometallic 2^+ to the bimetallic 3^{3+} and trimetallic 4^{5+} complexes, reflecting the effect of adding $Ru^{III}(py)_4Cl$ units.

The mononuclear complex 5^+ shows weaker but still intense bands in the visible that are probably also of LMCT character, despite the absence of a clear π-donor ligand. We assign these absorptions to transitions from the π orbitals of pyridine to the vacant dπ orbital of ruthenium(III). Because they are less intense than other LMCT bands, they are probably obscured by more intense LMCT transitions in other ruthenium(III) pyridine complexes. Similar features are observed in the spectrum of 1^+, together with a band shifted to the red that we assign to LMCT from chloride to ruthenium(III). The multinuclear complexes 6^{3+} and 7^{5+} also present a similar pattern, and the band intensities increase with the addition of ruthenium(III) acceptor units.

The complexes 6^{3+} and 7^{5+} show an additional band in the red at 13300 and 11000 cm⁻¹, respectively. The relatively low energy of these bands implies a transition from the highest-energy donor orbital to the lowest-energy acceptor orbital. Therefore, we assign these bands to LMCT from the chloride on the terminal ruthenium center to the $\{Ru^{III}(py)_4(CN)_2\}^+$ moiety. The latter is a much better acceptor than the terminal fragments, so these transitions are displaced to the red. This band is more intense in the trimetallic complex 7^{5+} and red-shifted, as expected for the presence of an extra $\{Ru^{III}(py)_4Cl\}^{2+}$ fragment. These "remote" transitions are due, possibly, to the extended mixing between the dπ orbitals along the intermetallic axis and are further evidence of the extended electronic communication in these compounds.

CONCLUSION

The contrasting structures of the trimetallic complexes 4^{2+} and 7^{2+} show that an eclipsed configuration, previously observed for 7^{2+}, is not heavily favored by electronic factors because it can be overcome by the forces involved in the crystal packing, as observed in 4^{2+}. Hence both configurations should be present in the solution experiments.

The spectroscopy and electrochemistry of the bi- and trimetallic complexes discussed here clearly show a substantial communication between the nearest- and next-nearest-neighbor ruthenium centers in these systems. Also, it is clear that this property can be enhanced by diminishing the energy gap between ruthenium units, as evidenced by the increased intensity of the MMCT transition and the larger split of the redox potential of the identical terminal ruthenium centers observed for the trimetallic complex where the py ligand in the central unit have been replaced by MeOpy.

It is worth mentioning the large values of H_{ab} estimated here for the next-nearest-neighbor ruthenium centers in the trimetallic complexes. Even larger H_{ab} values could be reached if the energy gap between the ruthenium centers is diminished. Those larger values would be compatible with charge delocalization, so a class III[48] multinuclear cyanide-bridged chain may be attainable.

The observed communication between the terminal ruthenium centers, together with the possibility of replacing the terminal chlorides with redox or photoactive units, suggests that these complexes can act as bridges that would allow energy or electron transfer between the terminal groups over significant and well-defined distances. Work is in progress in our group to explore such possibilities.

ASSOCIATED CONTENT

S **Supporting Information**

X-ray crystallographic data in CIF format, UV−visible and visible−NIR−IR spectra, and additional crystallographic data. This material is available free of charge via the Internet at http://pubs.acs.org.

AUTHOR INFORMATION

Corresponding Author
*E-mail: baraldo@qi.fcen.uba.ar.

Notes

The authors declare no competing financial interest.

ACKNOWLEDGMENTS

REFERENCES

(1) Baraldo, L. M.; Forlano, P.; Parise, A. R.; Slep, L. D.; Olabe, J. A. *Coord. Chem. Rev.* **2001**, *219*, 881.

(2) D'Alessandro, D. M.; Keene, F. R. *Chem. Rev.* **2006**, *106*, 2270.

(3) Dunbar, K. R.; Heintz, R. A. *Prog. Inorg. Chem.* **1997**, *45*, 283.

(4) Newton, G. N.; Nihei, M.; Oshio, H. *Eur. J. Inorg. Chem.* **2011**, *2011*, 3031.

(5) Vahrenkamp, H.; Geiss, A.; Richardson, G. N. *J. Chem. Soc., Dalton Trans.* **1997**, 3643.

(6) Catala, L.; Brinzei, D.; Prado, Y.; Gloter, A.; Stephan, O.; Rogez, G.; Mallah, T. *Angew. Chem., Int. Ed.* **2009**, *48*, 183.

(7) Culp, J. T.; Park, J.-H.; Frye, F.; Huh, Y.-D.; Meisel, M. W.; Talham, D. R. *Coord. Chem. Rev.* **2005**, *249*, 2642.

(8) Tanase, S.; Reedijk, J. *Coord. Chem. Rev.* **2006**, *250*, 2501.

(9) Ohba, M.; Okawa, H. *Coord. Chem. Rev.* **2000**, *198*, 313.

(10) Verdaguer, M.; Bleuzen, A.; Marvaud, V.; Vaissermann, J.; Seuleiman, M.; Desplanches, C.; Scuiller, A.; Train, C.; Garde, R.; Gelly, G.; Lomenech, C.; Rosenman, I.; Veillet, P.; Cartier, C.; Villain, F. *Coord. Chem. Rev.* **1999**, *192*, 1023.

(11) Coe, B. J.; Meyer, T. J.; White, P. S. *Inorg. Chem.* **1995**, *34*, 3600.

(12) In general, using differences in $\Delta E_{1/2}$ to compare mixing between sites in different mixed-valence systems is not appropriate because other factors also influence the magnitude of $\Delta E_{1/2}$, like electrostatic, inductive, resonance, or solvation effects. However, for closely related systems like the ones discussed here, one can assume that those factors remain mainly constant and, hence, an increase in $\Delta E_{1/2}$ indicates a larger mixing between the redox states.

(13) Timpson, C. J. Ph.D. Dissertation, University of North Carolina, Chapel Hill, NC, 1995.

(14) Coe, B. J.; Meyer, T. J.; White, P. S. *Inorg. Chem.* **1995**, *34*, 593.

(15) Albores, P.; Slep, L. D.; Weyhermuller, T.; Baraldo, L. M. *Inorg. Chem.* **2004**, *43*, 6762.

(16) Armarego, W. L. F.; Perrin, D. D. *Purification of Laboratory Chemicals*, 4th ed.; Butterworth-Heinemann: Oxford, U.K., 1996.

(17) Nagao, H.; Nishimura, H.; Kitanaka, Y.; Howell, F. S.; Mukaida, M.; Kakihana, H. *Inorg. Chem.* **1990**, *29*, 1693.

(18) Noviandri, I; Brown, K. N.; Fleming, D. S.; Gulyas, P. T.; Lay, P. A.; Masters, A. F.; Phillips, L. *J. Phys. Chem. B* **1999**, *103*, 6713.

(19) Kaim, W.; Fiedler, J. *Chem. Soc. Rev.* **2009**, *38*, 3373.

(20) *SCALE3 ABSPACK: Empirical Absorption Correction, CrysAlis — Software Package*; Oxford Diffraction Ltd.: Oxford, U.K., 2006.

(21) Sheldrick, G. M. *SHELXS97 and SHELXL97, Programs for Crystal Structure Resolution*; University of Göttingen: Göttingen, Germany, 1997.

(22) Spek, A. L. *Acta Crystallogr., Sect. D: Biol. Crystallogr.* **2009**, *65*, 148.

(23) Poddar, R. K.; Agarwala, U.; Manoharan, P. *J. Inorg. Nucl. Chem.* **1974**, *36*, 2275.

(24) Siddiqui, S.; Henderson, W. W.; Shepherd, R. E. *Inorg. Chem.* **1987**, *26*, 3101.

(25) Bendix, J.; Steenberg, P.; Søtofte, I. *Inorg. Chem.* **2003**, *42*, 4510.

(26) Toma, L.; Delgado, F.; Ruizperez, C.; Sletten, J.; Cano, J.; Clemente-Juan, J. M.; Lloret, F.; Julve, M. *Coord. Chem. Rev.* **2006**, *250*, 2176.

(27) Laidlaw, W. M.; Denning, R. G. *J. Chem. Soc., Dalton Trans.* **1994**, 1987−1994.

(28) Sheng, T. L.; Vahrenkamp, H. *Eur. J. Inorg. Chem.* **2004**, *43*, 1198.

(29) Richardson, G. N.; Brand, U.; Vahrenkamp, H. *Inorg. Chem.* **1999**, *38*, 3070.

(30) Geiss, A.; Vahrenkamp, H. *Eur. J. Inorg. Chem.* **1999**, 1793.

(31) Roncaroli, F.; Baraldo, L. M.; Slep, L. D.; Olabe, J. A. *Inorg. Chem.* **2002**, *41*, 1930.

(32) Albores, P.; Rossi, M. B.; Baraldo, L. M.; Slep, L. D. *Inorg. Chem.* **2006**, *45*, 10595.

(33) Rossi, M. B.; Abboud, K. A.; Albores, P.; Baraldo, L. M. *Eur. J. Inorg. Chem.* **2010**, 5613.

(34) Hush, N. S. *Prog. Inorg. Chem.* **1967**, *8*, 391.

(35) Hush, N. S. *Electrochim. Acta* **1968**, *13*, 1005.

(36) Mulliken, R. S. *J. Am. Chem. Soc.* **1952**, *74*, 811.

(37) Bignozzi, C. A. *J. Am. Chem. Soc.* **1985**, 1644.

(38) Bignozzi, C. A.; Scandola, F. *Inorg. Chem.* **1988**, 408.

(39) Cutin, E. H.; Katz, N. E. *Polyhedron* **1993**, *12*, 955.

(40) Scandola, F.; Argazzi, R.; Bignozzi, C. A.; Chiorboli, C.; Indelli, M. T.; Rampi, M. A. *Coord. Chem. Rev.* **1993**, *125*, 283.

(41) Watzky, M. A.; Macatangay, A. V.; VanCamp, R. A.; Mazzetto, S. E.; Song, X. Q.; Endicott, J. F.; Buranda, T. *J. Phys. Chem. A* **1997**, *101*, 8441.

(42) Macatangay, A. V.; Endicott, J. F. *Inorg. Chem.* **2000**, *39*, 437.

(43) Bublitz, G. U.; Laidlaw, W. M.; Denning, R. G.; Boxer, S. G. *J. Am. Chem. Soc.* **1998**, *120*, 6068.

(44) Brunschwig, B. S.; Creutz, C.; Sutin, N. *Chem. Soc. Rev.* **2002**, *31*, 168.

(45) Rocha, R. C.; Rein, F. N.; Jude, H.; Shreve, A. P.; Concepcion, J. J.; Meyer, T. J. *Angew. Chem., Int. Ed.* **2008**, *47*, 503.

(46) De Candia, A. G.; Singh, P.; Kaim, W.; Slep, L. D. *Inorg. Chem.* **2009**, *48*, 565.

(47) Lin, J.-L.; Tsai, C.-N.; Huang, S.-Y.; Endicott, J. F.; Chen, Y.-J.; Chen, H.-Y. *Inorg. Chem.* **2011**, *50*, 8274.

(48) Robin, M. B.; Day, P. *Adv. Inorg. Chem. Radiochem.* **1967**, *10*, 247.

(49) Kettle, S. F. A.; Diana, E.; Boccaleri, E.; Stanghellini, P. L. *Inorg. Chem.* **2007**, *46*, 2409.

(50) Pfennig, B. W.; Fritchman, V. A.; Hayman, K. A. *Inorg. Chem.* **2001**, *40*, 255.

(51) Concepcion, J. J.; Dattelbaum, D. M.; Meyer, T. J.; Rocha, R. C. *Philos. Trans. R. Soc., A* **2008**, *366*, 163.

(52) D'Alessandro, D. M.; Keene, F. R. *Chem. Soc. Rev.* **2006**, *35*, 424.